






Article

Swarm Satellite Magnetic Field Data Analysis Prior to 2019 Mw = 7.1 Ridgecrest (California, USA) Earthquake

Dedalo Marchetti ^{1,2} , Angelo De Santis ^{1,*} , Saioa A. Campuzano ^{1,†}, Maurizio Soldani ¹ , Alessandro Piscini ¹, Dario Sabbagh ¹ , Gianfranco Cianchini ¹, Loredana Perrone ¹  and Martina Orlando ¹

¹ Istituto Nazionale di Geofisica e Vulcanologia, Via di Vigna Murata 605, 00143 Rome, Italy; dedalo.marchetti@ingv.it (D.M.); saioa.arquero campuzano@ingv.it (S.A.C.); maurizio.soldani@ingv.it (M.S.); alessandro.piscini@ingv.it (A.P.); dario.sabbagh@ingv.it (D.S.); gianfranco.cianchini@ingv.it (G.C.); loredana.perrone@ingv.it (L.P.); orlandomartina93@gmail.com (M.O.)

² College of Instrumentation and Electrical Engineering, Jilin University, Changchun 130061, China

* Correspondence: angelo.desantis@ingv.it

† Now at Instituto de Geociencias IGEO (CSIC-UCM), c/Doctor Severo Ochoa, 7, Edificio Entrepabellones 7 y 8, Ciudad Universitaria, 28040 Madrid, Spain.

Received: 4 October 2020; Accepted: 13 December 2020; Published: 18 December 2020



Abstract: This work presents an analysis of the ESA *Swarm* satellite magnetic data preceding the Mw = 7.1 California Ridgecrest earthquake that occurred on 6 July 2019. In detail, we show the main results of a procedure that investigates the track-by-track residual of the magnetic field data acquired by the *Swarm* constellation from 1000 days before the event and inside the Dobrovolsky's area. To exclude global geomagnetic perturbations, we select the data considering only quiet geomagnetic field time, defined by thresholds on Dst and a_p geomagnetic indices, and we repeat the same analysis in two comparison areas at the same geomagnetic latitude of the Ridgecrest earthquake epicentre not affected by significant seismicity and in the same period here investigated. As the main result, we find some increases of the anomalies in the Y (East) component of the magnetic field starting from about 500 days before the earthquake. Comparing such anomalies with those in the validation areas, it seems that the geomagnetic activity over California from 222 to 168 days before the mainshock could be produced by the preparation phase of the seismic event. This anticipation time is compatible with the Rikitake empirical law, recently confirmed from *Swarm* satellite data. Furthermore, the *Swarm* Bravo satellite, i.e., that one at highest orbit, passed above the epicentral area 15 min before the earthquake and detected an anomaly mainly in the Y component. These analyses applied to the Ridgecrest earthquake not only intend to better understand the physical processes behind the preparation phase of the medium-large earthquakes in the world, but also demonstrate the usefulness of a satellite constellation to monitor the ionospheric activity and, in the future, to possibly make reliable earthquake forecasting.

Keywords: *Swarm*; earthquakes; Ridgecrest; ionospheric seismo-induced disturbances; earth magnetic field

1. Introduction

On 6 July 2019, at 03:19:53 UTC, an Mw = 7.1 earthquake happened in Southern California, Ridgecrest (35.770° N, 117.599° W), at a depth of 8.0 km. This event has been preceded by a large foreshock of magnitude 6.4 in about the same location (35.705° N, 117.506° W) on 4 July 2019 at 17:33:49 UTC. The tectonic location of these events is approximately 150 km northeast of the San Andreas Fault,

along the same direction and connected fault plane [1]. This region is seismically very active (e.g., [2]); we note that about 310 km northward with respect to the Ridgecrest epicentre, on 28 December 2016, three M5.5+ earthquakes happened in the same day (M5.6 at 16:18 UTC, M5.6 at 16:22 UTC and M5.5 at 17:14 UTC, respectively).

In this paper, we search for possible electromagnetic satellite signals before the earthquake occurrence. Fraser-Smith et al. [3] found a clear magnetic disturbance at the ground in the ULF band of 0.05 Hz–0.20 Hz prior to the M7.1 Loma-Prieta earthquake that occurred in California on 17 October 1989. The data were taken from a ground magnetic observatory, very close (7 km away) to the impending earthquake epicentre. Despite the promising observation that came from a ground observatory, it is still possible to search for this type of anomalies in magnetic satellite data.

Some of the first works that provided pieces of evidence in satellite data for electromagnetic disturbances that preceded the occurrence of earthquakes in the world came from the DEMETER satellite (e.g., [4–7]). In the last years, our research group has proposed some electromagnetic satellite anomalies from the European Space Agency (ESA) *Swarm* constellation, which is composed of three identical satellites in orbit from 22 November 2013 [8], and from the CSES-01 (China Seismo-Electromagnetic Satellite) dataset, prior to medium (M6.0–M7.4)–large (M7.5+) earthquakes in the world [9–14]. More recently, a Worldwide Statistical Correlation (WSC) analysis was applied on 4.7 years of *Swarm* magnetic field and electron density data, finding a significant correlation of concentrations of ionospheric anomalies with the worldwide shallow M5.5+ earthquakes in the same period [15]. Besides, they found that the largest concentrations of anomalies precede large earthquakes, with each anticipation time increasing with the magnitude of the seismic event, also confirming the Rikitake law [16] for electromagnetic pre-earthquake anomalies from satellite data.

A possible mechanism that could explain these pre-seismic disturbances was described by Freund [17], who supposed a release of positive holes on the fault that could alter the lithospheric electric circuit, producing a chain of electrical, mechanical and chemical alterations of the atmosphere up to the ionosphere. Other different mechanisms were, for example, described by Pulinets and Ouzounov [18], based on radon gas release in the preparation phase of large earthquakes.

In this work, we focus our attention on the Ridgecrest earthquake that occurred on 6 July 2019 and the possible electromagnetic anomalies detected by *Swarm* satellites during the preparation phase of the earthquake. This represents an extension of a recent paper [19] that analysed different physical quantities in the lithosphere, atmosphere and ionosphere, but here we are focusing especially on the magnetic field data of the *Swarm* mission. This paper is structured as follows: the first section presents data and methods used; the following section shows the results. Finally, we present some discussion and conclusions.

2. Data and Methods

We analysed the magnetic field data measured by the three identical satellites belonging to the *Swarm* constellation, called Alpha, Bravo and Charlie, respectively. They were launched by a single rocket on 22 November 2013 and are still in a quasi-polar orbit. After a few months of test, in-orbit calibration and commissioning, the satellites were put in the final orbital configuration: Alpha and Charlie fly almost in parallel at a lower orbit (in 2019 about 440 km above Earth surface) with a small separation of about 1.4 degrees, while the third satellite Bravo flies at a higher orbit (around 510 km in 2019) with a longitudinal shift that precedes along the mission time, and in 2019, it was about 90 degrees with respect to the orbit of the other two satellites. The orbital configuration was selected to take into account the different goals of the mission, mainly to measure the Earth's magnetic field and its variations, and in particular, to measure the Field Aligned Currents (FAC) and discriminate them from the lithospheric field.

The satellites are equipped by several instruments to measure the Earth's magnetic field, to monitor the ionospheric plasma environment and to determine the orbit and orientation of the satellites as best as possible (e.g., by Global Navigation Satellite Systems-GNSS, laser retroreflector, accelerometers).

In this work, we analysed the data of the Vector Field Magnetometer (VFM) and the Absolute Scalar Magnetometer (ASM) placed at the middle and at the end of a four-meter boom, respectively, both located at the back of each satellite. ESA downloads the raw data from *Swarm* satellites to the Kiruna and Svalbard stations and processes them in almost real-time (with a delay of 3–4 days only). The Agency provides calibrated magnetic open access data at Level 1b, where the measurements are provided not only in the instrumental frame but are also oriented in the Earth frame system NEC (North, East, Centre) at the original sampling frequency of 50 Hz (HR = High Resolution) and resampled at 1 Hz at the GPS o'clock seconds (LR = Low Resolution). In this work, we analysed the LR Magnetic *Swarm* product of all the satellites from 1000 days before the Ridgecrest mainshock. The data are provided with a quality check by means of 4 Flags: Flag_B and Flag_F are related to the quality of the measurement of each VFM magnetic field component and to ASM scalar intensity, respectively. Flag_attitude indicates if the pointing and attitude systems of satellites are working properly, and Flag_platform provides some information about the general status of the satellite platform, including, for example, the indication of the activation of the thrusters.

In order to extract magnetic anomalies possibly related to the major seismic events, we need to remove the main magnetic field. We then apply an approach successfully used in previous works and well described in the Methods section of [15] under the name of the MASS (MAGnetic *Swarm* anomaly detection by Spline analysis) algorithm. In particular, the magnetic field data are analysed by a numerical approximation of the temporal derivative, and then a cubic-spline is fitted and subtracted to remove the long trend. Finally, a moving window (generally of 7 degrees in latitude) investigates the obtained residuals.

The anomalies are defined by a threshold (named k_t) on the root mean square (rms) of the moving window compared with the Root Mean Square (RMS) of the whole track between -50° and $+50^\circ$ magnetic latitude. Only the tracks acquired in quiet geomagnetic field conditions ($|Dst| \leq 20$ nT and $a_p \leq 10$ nT) and with instruments and satellites in nominal conditions (checked by Flags) are taken into account to search for anomalies. Finally, the algorithm can also produce a figure of the residual of the magnetic measurements (X, Y, Z and F) of the track, together with some orbital information and geomagnetic indices Dst and a_p during the satellite passage. The epicentre of the earthquake and the Dobrovolsky's area (an approximation of the earthquake preparation area described in [20]), where we search for the electromagnetic anomalies, are automatically represented as well.

3. Results

Figure 1 reports the analysis performed by the MASS algorithm of the magnetic data from *Swarm* Bravo track 5 acquired on 6 July 2019. The figure shows a map (in panel e) with the Earth's surface projection of the satellite track; the colour is related to Flags: brown when the VFM instrument and satellite are in nominal condition, or light blue when Flag_attitude is equal to 18 (and the others are nominal). We note that this track preceded the earthquake occurrence by about 15 min. It presents two highlighted behaviours in the Y magnetic field component (panel b), underlined by a red circle and an orange one. The red circled anomaly is closer to the latitude of the earthquake, and it is entirely inside the Dobrovolsky's area (yellow circle on the map). The geomagnetic field conditions during this time were sufficiently quiet ($Dst = 2$ nT, $a_p = 4$ nT, AE without particular activity during and in the hours before—as well as the Dst and a_p —the passage of the satellite above the investigated region, so excluding any possible penetrating electric field from the auroral regions). All the samples are acquired with Flags that indicate data of good quality for science, as indicated by ESA [21]. As marked in Figure 1, the flagged sections of the track (in light blue in panel e) are due to a bright object (e.g., the Sun) in one of the three-star cameras. The other two cameras were nominal, and no other issues were detected on this track, so we confirm that all the samples can be considered good for the purpose of the present paper (as two cameras are more than sufficient to properly rotate the data from the instrument to NEC frame).

The *Swarm* Alpha, Bravo and Charlie Y magnetic field component data have been systematically analysed. Here we have enough data to extend back the analysis until 1000 days before the earthquake, i.e., from 10 October 2016 to 6 July 2019.

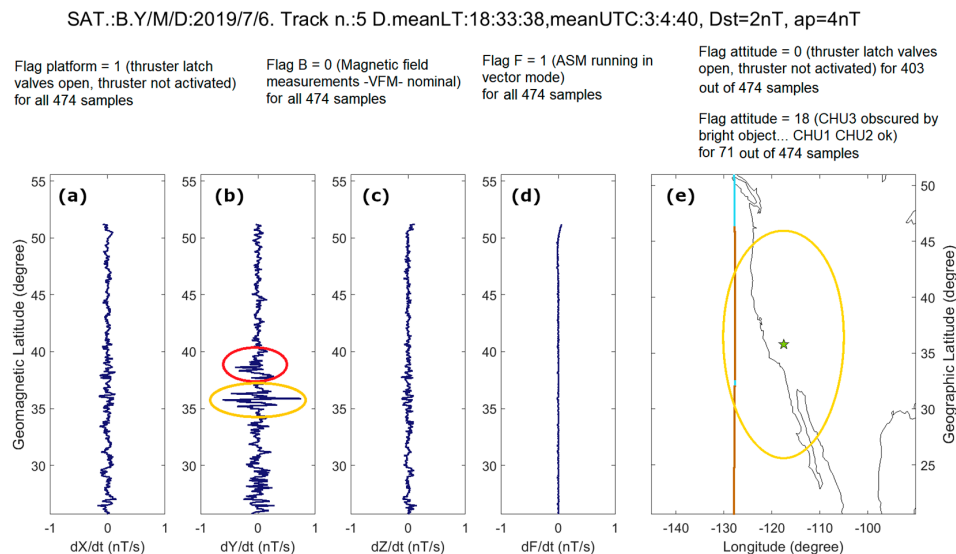


Figure 1. Magnetic data from *Swarm* Bravo track number 5 on 6 July, 2019. The track preceded the earthquake occurrence by about 15 min. Panels (a–d) show the residuals for first differences of X, Y, Z and absolute scalar intensity of the magnetic field, respectively. Panel (e) represents a geographical map of the investigated region, with the projection of the satellite track (the colour is related to Flag conditions), the epicentre of the Ridgecrest earthquake (green star) and the Dobrovolsky's area (yellow circle). The red and orange circles underline two disturbances on the Y component of the magnetic field. Some detailed information about the Flags related to this track is also provided.

As significant concentrations of anomalies were found in the closest 3.34 degrees from the epicentre of the earthquakes by De Santis et al. [15], we decided to select a circular area of the same extension around the California earthquake. We applied the MASS algorithm, and for the analysis, we selected a threshold of $k_t = 2.5$ within the sliding window of the 7-degree length in latitude.

Figures 2 and 3 show the cumulative number of *Swarm* Alpha, Bravo and Charlie anomalies in a circular area of 3.34 degrees around the $M_w = 7.1$ California 2019 epicentre (blue line) compared with other validation areas in the US East Coast and Europe (EU), respectively, at the same magnetic latitude (red line) and with the same extension centred on geographic coordinates 32.92° N, 82.5° W and 39.45° N, 3.30° W, respectively. The comparison regions have been chosen on a similar context (i.e., above continental areas and so excluding fully oceanic ones) in order to compare potential similarities surely not due to California earthquake. We checked that in both comparison areas, and United States Geological Survey (USGS) reports no $M_{4.5+}$ earthquakes during the analysed time (i.e., from 10 October 2016 to 6 July 2019).

The cumulative number of anomalies around the earthquake epicentre presents several changes of slope that underline probably a particular geomagnetic activity, despite the fact that the data are selected only in quiet geomagnetic field time. Indeed, most of these behaviours happened also in the comparison areas, in some cases with some delay. In particular, the part of the cumulates between -600 and -500 days presents a very similar behaviour in all the considered areas (and an even steeper increase in the US East Coast around 550 days before the earthquake), pointing to a global effect affecting all the analyses. When the slope-change in the cumulate happens in all the areas, we can exclude a possible relationship with the impending seismic event and attribute this behaviour to some global (but small) perturbations of geomagnetic field, or at least those located in the Northern hemisphere. For this reason, even if there are two strong increases of anomalies at around -500 and

−365 days (well visible also from the difference of the cumulates shown in Figures 2b and 3b), we tend to exclude a relationship with the preparation of the incoming earthquake. However, it is worth noting that for both periods (around 500 and 365 days before) the number of anomalies (i.e., the jump in cumulate) over the epicentral area is higher than over the EU comparison one, but in the US East Coast, this is not verified. Moreover, the slope-changes in the cumulative number of anomalies over California from −222 to −167 days (highlighted by two data tips in Figures 2a and 3a) and not present over the two comparison areas could be related to the preparatory phase of the California Ridgecrest earthquake. Furthermore, we checked if the anticipation time is compatible with the Rikitake law estimated for *Swarm* magnetic field data by De Santis et al. [15]. This empirical law is a linear relationship between the decimal logarithm of the anticipation time (ΔT expressed in days) and the earthquake magnitude (M) as $\log(\Delta T) = a + b \cdot M$, where a and b are the two coefficients of the linear fit. For the increase of anomalies around the California earthquake highlighted in Figure 2, the logarithm of its anticipation time is around 2.2–2.3. De Santis et al. [15] estimated the same value for an $M_w = 7.1$ earthquake, as $\log_{10}(\Delta T) = 2.7 (\pm 1.8)$. Therefore, the detected anticipation time for the California earthquake is statistically compatible with the value already estimated. It is important to note that even if the analysed satellites are the same, the time period of this earthquake was not included in the statistical analysis provided by De Santis et al. [15], which included data until August 2018, so we can consider the present result a further validation.

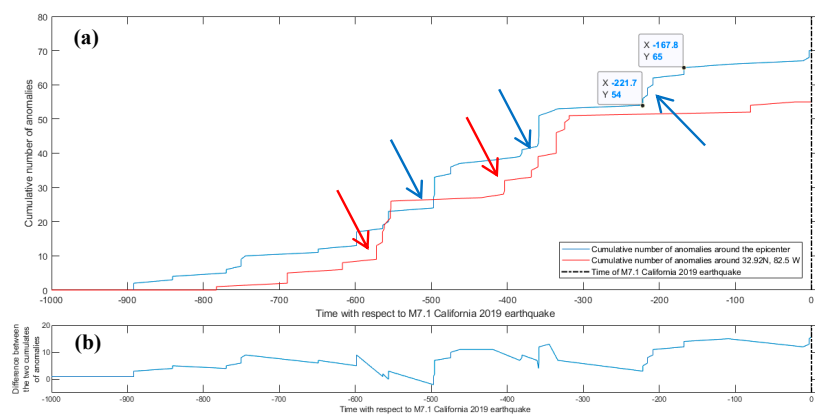


Figure 2. (a) Cumulative number of anomalies in a circular area of 3.34 degrees around the M7.1 California 2019 epicentre (blue line) compared with a comparison area on the opposite coast side of the US at the same magnetic latitude and with the same extension (red line). The arrows indicate the principal jumps discussed in the main text with the same colour of the cumulate curve. (b) Difference between the two cumulates.

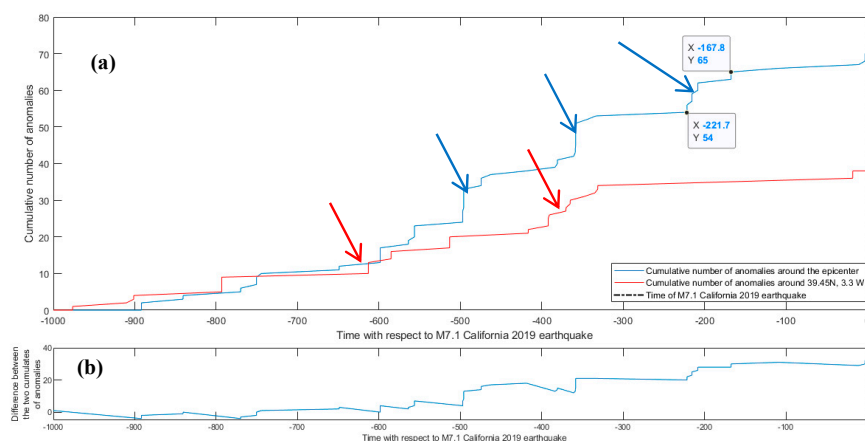


Figure 3. The same as Figure 2 but using a comparison area in Europe (Spain) centred at 3.3° W longitude and the same geomagnetic latitude of the epicentre (i.e., 39.45° N geographic latitude). (a) Cumulative number of anomalies; (b) Difference between the two cumulates.

To further check the detected anomalies, we propose to calculate the percentage of anomalies in the California area with respect to the ones in the comparison (US and EU) areas, normalised with respect to the potential tracks by the following expression:

$$\% = \frac{(\text{anomalies}_{\text{California}} - \text{anomalies}_{\text{comparison}})}{\text{anomalies}_{\text{comparison}}} \cdot \frac{\text{Total Windows}_{\text{comparison}}}{\text{Total Windows}_{\text{California}}}$$

The “total windows” are the number of windows whose centres fall inside the investigated area during the quiet geomagnetic time. Table 1 summarises these values for each satellite and for the constellation as a whole. We noticed that the constellation presented more anomalies in the epicentral area with a normalised percentage from about 27% to 82%. The single satellite generally shows more anomalies in the epicentral area with respect to the comparison ones, with the exception of Alpha, which presents 22% less anomalies in the epicentral area with respect to the US East Coast comparison one. In the other cases, the satellites present more anomalies in the epicentral area with a normalised percentage from 42% up to 220%. Charlie is the satellite with the highest percentage of anomalies in the epicentral area with respect to both comparison ones. All the differences between the California and EU areas, reported in Table 1, are statistically significant. Considering all the satellites, in the epicentral area, the number of anomalies is 15 more than in the US East Coast comparison area and 32 more than in EU one, which corresponds to 27% and 82% more, respectively.

Table 1. Number of anomalies, total windows and normalised percentage of anomalies detected in the epicentral area with respect to (w.r.t.) the comparison areas centred in US East Coast and in Europe, using the *Swarm* satellites. The anomalies have been obtained by considering 1000 days before the California earthquake that occurred on 6 July 2019.

	Alpha		Bravo		Charlie		All	
	Anomalies	Total Windows	Anomalies	Total Windows	Anomalies	Total Windows	Anomalies	Total Windows
California area	20	1268	24	1138	26	1033	70	3439
Comparison area (US East Coast)	26	1210	14	1186	15	1000	55	3396
Normalised percentage of anomalies w.r.t. US comparison area	−22.0%		74.4%		71.0%		26.9%	
Comparison area (Europe)	6	1193	14	1203	18	971	38	3367
Normalised percentage of anomalies w.r.t. Europe comparison area	219.5%		75.5%		41.8%		82.4%	

We also compared the distribution of the anomalies with respect to their local time in all the areas. A difference in local time distribution can be considered to support the possible link with the seismic activity. In particular, we checked whether the anomalies are concentrated at a particular time of the day. To be sure that any possible conclusion will not be affected by the influence of the *Swarm* constellation orbital parameters on the local time, the latter has been checked by analysing how it is distributed in the analysed period, as shown in Figure 4a. All the analysed windows with quiet geomagnetic field conditions (as above defined) are reported as dots: the colours for Alpha and Charlie satellites have been chosen to be the same for simplicity, considering that their local time differences are few minutes. The local time distribution of the analysed window confirms that the epicentral and comparison areas are equally covered for the same period. Figure 4b–d report the local

time histogram distributions of the detected anomalies for the California area, US East Coast and EU regions. It is evident that in the epicentral area, there are more anomalies in “early morning” between 2 AM and 8 AM with respect to the comparison areas, where the anomalies are mainly distributed at midday (US East Coast), and at sunset and in the first hours after for both comparison areas. We can consider that even the different distribution in the local time of the anomalies can be a sign of different phenomena that produce these anomalies.

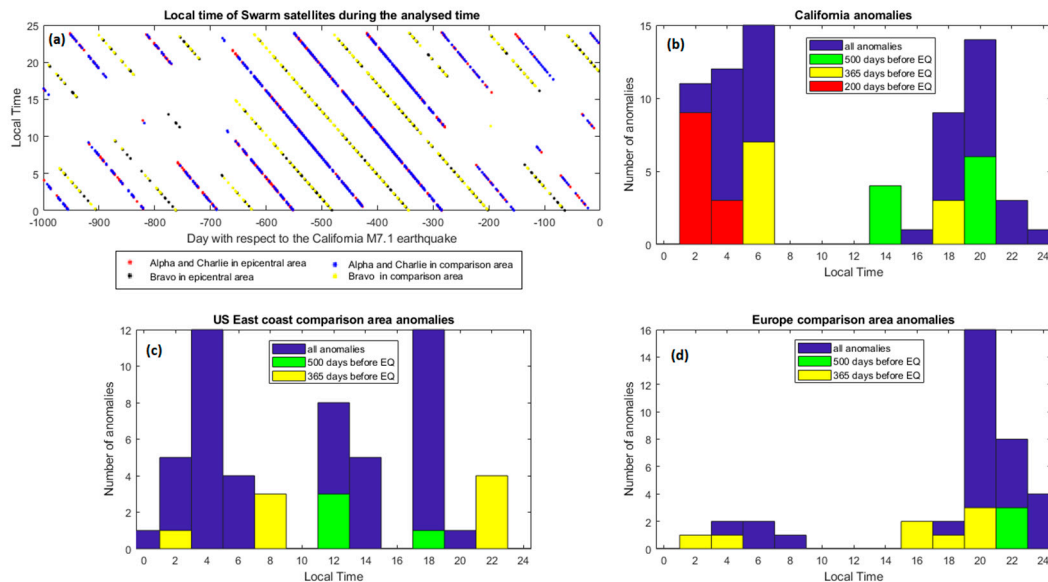


Figure 4. Local time distribution of the analysed windows. (a) Passages of the three satellites above the area in geomagnetic field quiet time; (b) local time distribution of the anomalies in the earthquake area; (c,d) local time distribution of the anomalies in the US East Coast and Europe comparison areas, respectively. The histograms in panels (b–d) highlight the anomalies around the jumps indicated by the coloured arrows in Figures 2a and 3a.

For the principal three jumps (indicated by coloured arrows in Figures 2a and 3a) in the cumulative number of anomalies at around 500, 365 and 200 days before the earthquake in the epicentral and comparison areas, the local time distribution has been depicted by different colour bars in the histograms. For both comparison areas, no anomalies have been detected 200 days before the earthquake. We noted that at 14 local time, in the epicentral area, some anomalies (4 over 10) have been detected 500 days before the event, but for the US East Coast, 3 anomalies have been detected 2 h before, proposing this as a regional non-seismic phenomenon.

4. Discussion and Conclusions

By an automatic analysis of the anomalous *Swarm* three-satellite tracks, it has been possible to detect an increase of anomalies around 200 days before the 6 July 2019 California mainshock. Such an increase of anomalies is considered as possibly related to the preparatory phase of the California Ridgecrest earthquake. The result has been validated after comparison with two equivalent areas centred at the same geomagnetic latitude and with a longitude that corresponds to US East Coast (82.5° W) and to Europe–Spain (3.3° W). The comparison is essential to exclude possible global perturbations of the geomagnetic field. The detected anticipation times are well compatible with those expected by the Rikitake empirical law, recently confirmed for satellite data by the statistical studies conducted by De Santis et al. [15].

Other increments of anomalies have been detected at about 500 and 365 days before the earthquake, but increases of the cumulates have also been detected in the comparison regions at similar times. We noted that such increases at about 500 and 365 days in the US East Coast comparison area are

even higher than above epicentral area. This made us conclude that these anomalies are a regional phenomenon in US, but it is not likely due to the preparation phase of the Ridgecrest earthquake.

An open question is whether only one type of pre-earthquake Lithosphere–Atmosphere–Ionosphere Coupling (LAIC) process exists or whether more phenomena could be involved during the earthquake preparation phase. The latter hypothesis seems to be more reliable, possibly explaining why some anomalies are closer in time to the event. In this paper, a magnetic anomaly in the Y component appears 15 min before the mainshock, while similar anomalies appear 9 days before the 2016 M7.8 Ecuador earthquake and 3 days before the 2016 M6.0 Italy earthquake, as found by Akhoondzadeh et al. [10] and Marchetti et al. [12], respectively.

For the same earthquake, De Santis et al. [19] found a chain of Lithosphere–Atmosphere–Ionosphere anomalies even increasing in number toward the event. This work is complementary in the sense that the anomalies depicted in this paper covered the whole preparation phase investigated in De Santis et al. [19], with some anomalies with long anticipation time (Figures 2 and 3) until an early anomaly before the earthquake (shown in Figure 1).

It is worth noting that the coverage of the three *Swarm* satellites is not uniform in time, so the analysed region is revisited from each satellite about twice per day (one during night-time and the other one in the daytime). Therefore, a broader satellite constellation could hopefully permit us to have more chances to detect such phenomena, and to have better time coverage worldwide, i.e., all the active seismic zones.

The higher number of anomalies in the epicentral area with respect to the comparison ones suggests that at least some of the anomalies in the epicentral area could be due to the earthquake preparation phase. This result is similar to that obtained in the previous investigation conducted by De Santis et al. [14,15] in the frame of the ESA funded project SAFE (SwArm For Earthquake study). Moreover, the concentration of anomalies in a different local time with respect to those detected in the comparison areas can be considered a further hint in supporting this hypothesis.

The presented analyses not only intend to better understand the physical processes behind the preparation phase of the medium-large earthquakes in the world but also to demonstrate the usefulness of a large satellite constellation to monitor the ionospheric geomagnetic activities and to investigate how long a seismo-induced ionospheric disturbance could be detected in the active seismic region before the event, which can be even several months before the mainshock. Finally, this type of analysis, together with lithospheric, geochemical and atmospheric data investigation, could possibly bring, in the near future, the capability to make reliable earthquake forecasting.

Author Contributions: Conceptualization, D.M. and A.D.S.; Data curation, D.M.; Formal analysis, D.M.; Funding acquisition, A.D.S.; Investigation, D.M. and A.D.S.; Methodology, D.M., A.D.S., S.A.C. and D.S.; Project administration, A.D.S.; Software, D.M., S.A.C. and G.C.; Supervision, A.D.S. and L.P.; Validation, S.A.C., M.S., A.P., D.S., G.C., L.P. and M.O.; Visualization, D.M., S.A.C., M.S., D.S. and M.O.; Writing—original draft, D.M. and A.D.S.; Writing—review & editing, D.M., A.D.S., S.A.C., M.S., A.P., D.S., G.C. and M.O. All authors have read and agreed to the published version of the manuscript.

Funding: This research was funded by European Space Agency in the framework of the ESA-funded project SAFE (“*Swarm* for Earthquake study”, Contract No. 4000116832/15/NL/MP), its extension e-SAFE (Contract No. 4000113862/15/NL/MP) and also by Italian Space Agency (ASI) with the project “LIMADOU-Scienza” (Contract No. 2016-16-H0) and ISSI-BJ project “The electromagnetic data validation and scientific application research based on CSES satellite”. The APC was provided by FURTHER (“The role of fluids in the preparatory phase of earthquakes in Southern Apennines”) project funded by INGV Earthquake Department.

Acknowledgments: The authors are very grateful for the useful comments received by two anonymous reviewers that permitted us to improve the quality of our work and research investigation.

Conflicts of Interest: The authors declare no conflict of interest. The funders had no role in the design of the study; in the collection, analyses, or interpretation of data; in the writing of the manuscript, or in the decision to publish the results.

References

1. USGS, U.S. Geological Survey; National Earthquake Information Center. M 7.1—2019 Ridgecrest Earthquake Sequence. 2019. Available online: <https://earthquake.usgs.gov/earthquakes/eventpage/ci38457511/executive> (accessed on 16 July 2019).
2. Giardini, D.; Gruenthal, G.; Shedlock, K.M.; Zhang, P. 74—The GSHAP global seismic hazard map. *Int. Geophys.* **2003**, *81*, 1233–1239. [[CrossRef](#)]
3. Fraser-Smith, A.C.; Bernardi, A.; McGill, P.R.; Ladd, M.E.; Helliwell, R.A.; Villard, O.G., Jr. Low-frequency magnetic field measurements near the epicenter of the Ms7.1 Loma Prieta Earthquake. *Geophys. Res. Lett.* **1990**, *17*, 1465–1468. [[CrossRef](#)]
4. Parrot, M.; Berthelier, J.J.; Lebreton, J.P.; Sauvaud, J.A.; Santolík, O.; Blecki, J. Examples of unusual ionospheric observations made by the DEMETER satellite over seismic regions. *Phys. Chem. Earth* **2006**, *31*, 486–495. [[CrossRef](#)]
5. Němec, F.; Santolík, O.; Parrot, M.; Berthelier, J.-J. Spacecraft observations of electromagnetic perturbations connected with seismic activity. *Geophys. Res. Lett.* **2008**, *35*, 05109. [[CrossRef](#)]
6. Píša, D.; Němec, F.; Santolík, O.; Parrot, M.; Rycroft, M.J. Additional attenuation of natural VLF electromagnetic waves observed by the DEMETER spacecraft resulting from preseismic activity. *J. Geophys. Res. Space Phys.* **2013**, *118*, 5286–5295. [[CrossRef](#)]
7. Yan, R.; Parrot, M.; Pinçon, J.-L. Statistical Study on Variations of the Ionospheric Ion Density Observed by DEMETER and Related to Seismic Activities. *J. Geophys. Res. Space Phys.* **2017**, *122*. [[CrossRef](#)]
8. Friis-Christensen, E.; Lühr, H.; Hulot, G. Swarm: A constellation to study the Earth's magnetic field. *Earth Planets Space* **2006**, *58*, 351–358. [[CrossRef](#)]
9. De Santis, A.; Balasis, G.; Pavón-Carrasco, F.J.; Cianchini, G.; Manda, M. Potential earthquake precursory pattern from space: The 2015 Nepal event as seen by magnetic Swarm satellites. *Earth Planet. Sci. Lett.* **2017**, *461*, 119–126. [[CrossRef](#)]
10. Akhoondzadeh, M.; De Santis, A.; Marchetti, D.; Piscini, A.; Cianchini, G. Multi precursors analysis associated with the powerful Ecuador (MW 7.8) earthquake of 16 April 2016 using Swarm satellites data in conjunction with other multi-platform satellite and ground data. *Adv. Space Res.* **2018**, *61*, 248–263. [[CrossRef](#)]
11. Akhoondzadeh, M.; De Santis, A.; Marchetti, D.; Piscini, A.; Jin, S. Anomalous seismo-LAI variations potentially associated with the 2017 Mw = 7.3 Sarpol-e Zahab (Iran) earthquake from Swarm satellites, GPS-TEC and climatological data. *Adv. Space Res.* **2019**, *64*, 143–158. [[CrossRef](#)]
12. Marchetti, D.; De Santis, A.; D'Arcangelo, S.; Poggio, F.; Jin, S.; Piscini, A.; Campuzano, S.A. Magnetic Field and Electron Density Anomalies from Swarm Satellites Preceding the Major Earthquakes of the 2016–2017 Amatrice-Norcia (Central Italy) Seismic Sequence. *Pure Appl. Geophys.* **2020**, *177*, 305–319. [[CrossRef](#)]
13. Marchetti, D.; De Santis, A.; Shen, X.; Campuzano, S.A.; Perrone, L.; Piscini, A.; Di Giovambattista, R.; Jin, S.; Ippolito, A.; Cianchini, G.; et al. Possible Lithosphere-Atmosphere-Ionosphere Coupling effects prior to the 2018 Mw = 7.5 Indonesia earthquake from seismic, atmospheric and ionospheric data. *J. Asian Earth Sci.* **2020**, *188*, 104097. [[CrossRef](#)]
14. De Santis, A.; Marchetti, D.; Spogli, L.; Cianchini, G.; Pavón-Carrasco, F.J.; De Franceschi, G.; Di Giovambattista, R.; Perrone, L.; Qamili, E.; Cesaroni, C.; et al. Magnetic Field and Electron Density Data Analysis from Swarm Satellites Searching for Ionospheric Effects by Great Earthquakes: 12 Case Studies from 2014 to 2016. *Atmosphere* **2019**, *10*, 371. [[CrossRef](#)]
15. De Santis, A.; Marchetti, D.; Pavón-Carrasco, F.J.; Cianchini, G.; Perrone, L.; Abbattista, C.; Alfonsi, L.; Amoruso, L.; Campuzano, S.A.; Carbone, M.; et al. Precursory worldwide signatures of earthquake occurrences on Swarm satellite data. *Sci. Rep.* **2019**, *9*, 1–13. [[CrossRef](#)] [[PubMed](#)]
16. Rikitake, T. Earthquake precursors in Japan: Precursor time and detectability. *Tectonophysics* **1987**, *136*, 265–282. [[CrossRef](#)]
17. Freund, F. Pre-earthquake signals: Underlying physical processes. *J. Asian Earth Sci.* **2011**, *41*, 383–400. [[CrossRef](#)]
18. Pulinet, S.A.; Ouzounov, D. Lithosphere–Atmosphere–Ionosphere Coupling (LAIC) model. an unified concept for earthquake precursors validation. *J. Asian Earth Sci.* **2011**, *41*, 371–382. [[CrossRef](#)]

19. De Santis, A.; Cianchini, G.; Marchetti, D.; Piscini, A.; Sabbagh, D.; Perrone, L.; Campuzano, S.A.; Inan, S. A Multiparametric Approach to Study the Preparation Phase of the 2019 M7.1 Ridgecrest (California, United States) Earthquake. *Front. Earth Sci.* **2020**, *8*. [[CrossRef](#)]
20. Dobrovolsky, I.P.; Zubkov, S.I.; Miachkin, V.I. Estimation of the size of earthquake preparation zones. *Pure Appl. Geophys.* **1979**, *117*, 1025–1044. [[CrossRef](#)]
21. Gil, C.; Tøffner-Clausen, L.; Olsen, N.; Igino Coco, I.; Qamili, E.; Ottavianelli, G. Swarm Level 1b Flags Usage and Interpretation. 3rd Swarm Cal/Val Meeting. 18 June 2014. Available online: <https://earth.esa.int/documents/10174/1514862/Swarm-Level-1b-flags-usage-interpretation> (accessed on 10 July 2019).

Publisher’s Note: MDPI stays neutral with regard to jurisdictional claims in published maps and institutional affiliations.



© 2020 by the authors. Licensee MDPI, Basel, Switzerland. This article is an open access article distributed under the terms and conditions of the Creative Commons Attribution (CC BY) license (<http://creativecommons.org/licenses/by/4.0/>).